Stress Analysis of 3D Generally Anisotropic Elastic Solids Using the Boundary Element Method

C. L. Tan[1], Y.C. Shiah[2] and C.W. Lin[2]

Abstract: The explicit, closed-form expressions of the Green's functions for generally anisotropic elastic solids in three-dimensions that have been derived using Stroh's formalism are employed in a formulation of the boundary element method (BEM). Unlike several other existing schemes, the evaluation of these fundamental solutions does not require further numerical integration in the BEM algorithm; they have surprisingly not been implemented previously. Three numerical examples are presented to demonstrate the veracity of the implementation and the general applicability of the BEM for the 3D elastic stress analysis of generally anisotropic solids. The results are compared with known solutions in the literature where possible, or those obtained by another numerical method, namely, the finite element method; in all cases, very good agreement is shown to be achieved.

Keywords: Fundamental solutions, Green's functions, anisotropic elasticity, Stroh's eigenvalues, boundary integral equations, boundary element method.

1 Introduction

The determination of accurate stress distributions in structural details such as those near stress concentrations is very important in the design and safe-life assessment of many engineering components. To this end, the boundary element method (BEM) is well recognized as a very efficient numerical tool for the linear elastic stress analysis of isotropic solids (see, e.g. Aliabadi, 2002). This is also true for treating problems of anisotropic solids in two-dimensions (see, e.g. Tan and Gao, 1992; Tan, *et al.*, 1992; Shiah and Tan, 2000; Shiah, *et al.*, 2006). However, the advances that have been made of this method on its application to three-dimensional (3D) anisotropic elastic solids had been rather limited and quite sporadic. This is in spite of the increasing use of such materials in engineering over the past few decades. Thus, the finite element method remains a popular numerical tool for treating 3D

---

[1] Dept. of Mechanical and Aerospace Engineering, Carleton University, Ottawa, Canada K1S 5B6
[2] Dept. of Aerospace and Systems Engineering, Feng Chia University, Taichung, Taiwan, R.O.C.

anisotropic elastic solids despite some of its drawbacks. In this regard, the other techniques that have also been employed include the strip element method (Li and Achenbach, 1994), and the finite difference method (Paik *et al.*, 2004); meshless methods have been developed for 2D anisotropic elasticity (see, e.g., Sladek, *et al.*, 2004; Li and Atluri, 2008) as well, but to a much lesser extent for the 3D case.

The main reason for the relatively slow pace of development of the BEM for 3D anisotropic elasticity is the mathematical complexity of the fundamental solutions to the governing equations. These fundamental solutions, or Green's functions, are a necessary item in the formulation of the boundary integral equation (BIE). An efficient and accurate means of evaluating them is a key to the successful implementation of the BEM, as well as of other numerical techniques (such as the method of fundamental solutions and the meshless local BIE method). The fundamental solution of the displacement field due to a unit point load in a 3D generally anisotropic infinite solid in elastostatics has been derived by Lifschitz and Rozentsweig (1947). It was expressed as a contour integral around a unit circle and its integrand contains the Christoffel tensor defined in terms of the elastic material constants. No closed-form expression for this Green's function was available for the generally anisotropic case. Thus, the focus of several investigators over the past several decades has been to evaluate this integral and its derivatives into as simple and explicit an analytical form as possible (see, e.g., Synge, 1957; Barnett, 1972; Ting and Lee, 1997; Nakamura and Tanuma, 1997; Wang, 1997; and Lee, 2003). The development of computationally efficient schemes for their numerical evaluation has also been a subject of several investigations in the context of BEM development (see, e.g., Wilson and Cruse, 1978; Chen and Lin, 1995; Sales and Gray, 1998; Tonon *et al.*, 2001; Pan and Yuan, 2000; Phan *et al.*, 2004; and Wang and Denda, 2007).

A numerical formulation of the BEM for 3D stress analysis of a generally anisotropic solid was first implemented by Wilson and Cruse (1978). In their algorithm, the contour integral in the Green's function of Lifschitz and Rozentsweig (1947) is numerically evaluated for a given material, and a large database of numerically evaluated point load solutions and their derivatives is generated. Interpolation of these pre-calculated values is performed in the BEM calculations. It is, however, computationally quite demanding and its accuracy for highly anisotropic materials may also be questionable. Sales and Gray (1998) improved significantly on the efficiency of the Wilson-Cruse approach by transforming the integrand of the line integral for the Green's function into a rational function using the method of residues. A concern of the Sales–Gray algorithm on its numerical instability when there are multiple poles of the residue was overcome by Phan *et al.*(2004). There was no report of any implementation into a BEM algorithm in these works, how-

ever. Tonon *et al.* (2001) have also developed a BEM formulation for 3D generally anisotropic media. It is based on the theoretical solution of the Green's function for displacements derived by Wang (1997) who employed the Radon transform and the calculus of residues to derive an explicit algebraic expression for the fundamental solution. The algorithm to compute the fundamental solution involves contour integration over a rectangular parallelepiped; it is arguably quite complex and cumbersome. Their implementation was verified by some very simple numerical examples in the paper. Recently, Wang and Denda (2007) have also developed a 3D BEM algorithm in which the fundamental solution is expressed in terms of a line integral over a semi-circle instead. Flat triangular boundary elements are employed in their formulation, and the Green's function is analytically integrated over each of these flat elements to obtain the system matrices.

An alternative, explicit algebraic form of the fundamental solution for the displacements and its derivatives in a 3D anisotropic body has also been presented by Ting and Lee (1997) and Lee (2003), respectively. They can be expressed primarily in terms of Stroh's eigenvalues which are the only quantities that need to be numerically solved for. Being explicit in algebraic form, these fundamental solutions can be numerically evaluated in a fairly straightforward manner; this has been demonstrated very recently by Shiah *et al.* (2008a, b). Surprisingly, it is only very recently that the BEM formulation utilizing these explicit-form fundamental solutions has been reported and even then, only for the special case of transverse isotropy (Tavara *et al.*, 2008). Indeed, as has been noted by Tavara *et al.* (2008) as well, to the present authors' knowledge, no BEM formulation employing them has hitherto been published in the literature.

In this paper, the explicit-form fundamental solutions for the displacements and its derivatives by Ting and Lee (1997) and Lee (2003) are used in the conventional BEM formulation for the general case of 3D elastic anisotropy. The implementation has been successfully carried out by modifying a BEM code based on the quadratic isoparametric element formulation that has been previously developed for 3D isotropic elastostatics (Tan and Fenner, 1978, 1979; Tan, 1983). In the following sections, the fundamental solutions employed will first be reviewed. Some aspects of the numerical implementation into the BEM code will also be discussed. This will then be followed by three examples, including test problems and those with stress concentrations.

2 Anisotropic fundamental solutions

The details of the derivation of the BIE in elastostatics are well documented in the literature and hence will not be reviewed here. The BIE is an integral constraint equation which relates the displacements u_j and tractions t_j at the surface S of the

homogeneous elastic domain. It may be written in indicial notation as

$$C_{ij}u_i(P) + \int_S u_i(Q)T^*_{ij}(P,Q)dS = \int_S t_i(Q)U_{ij}(P,Q)dS + \int_\Omega X_i(q)U_{ij}(P,q)d\Omega \qquad (1)$$

where the leading coefficient $C_{ij}(P)$ depends upon the local geometry of S at the source point P; $U_{ij}(P,Q) \equiv \mathbf{U}(\mathbf{x})$, and $T^*_{ij}(P,Q)$ represent the fundamental solutions of displacements and tractions, respectively, in the x_i-direction at the field point Q due to a unit load in the x_j-direction at P in a homogeneous infinite body. For a generally anisotropic material, the point load solution for the displacement field may be written as (Barnett, 1972; Synge, 1957)

$$U_{ij} = \frac{1}{8\pi^2 r} \int_0^{2\pi} \mathbf{Z}^{-1} d\psi, \qquad (2)$$

where r is the radial distance between the source point P at the local origin $\mathbf{x} = 0$ and the field point Q at $\mathbf{x} = (x_1, x_2, x_3)$. In eq. (2), the integral is taken around the unit circle $|\mathbf{n}^*| = 1$ on the oblique plane normal to $\mathbf{x}_Q$; the unit vector $\mathbf{n}^*$ on the oblique plane can be written in terms of an arbitrary parameter ψ as

$$\mathbf{n}^* = \mathbf{n}\cos\psi + \mathbf{m}\sin\psi m \qquad (3)$$

where the vectors $\mathbf{n}$, $\mathbf{m}$ along with $\mathbf{x}/r$ form a right-handed triad $[\mathbf{n}, \mathbf{m}, \mathbf{x}/r]$. With reference to Figure 1, the general form of $\mathbf{n}$ and $\mathbf{m}$ can be expressed as

$$\mathbf{n} = (\cos\phi\cos\theta, \ \cos\phi\sin\theta, \ -\sin\phi), \quad \mathbf{m} = (-\sin\theta, \ \cos\theta, \ 0), \qquad (4)$$

where $0 \le \theta < 2\pi$ and $-\pi/2 \le \phi \le \pi/2$.

The integrand $\mathbf{Z}^{-1}$ in eq. (2) is the inverse matrix of $\mathbf{Z} \equiv Z_{ij}$ which can be expressed as (Ting and Lee, 1997)

$$Z_{ik}(\psi) = C_{ijks}(n_j\cos\psi + m_j\sin\psi)(n_s\cos\psi + m_s\sin\psi). \qquad (5)$$

where $C_{ijks} \equiv \mathbf{C}$ is the elastic stiffness tensor of the anisotropic material.

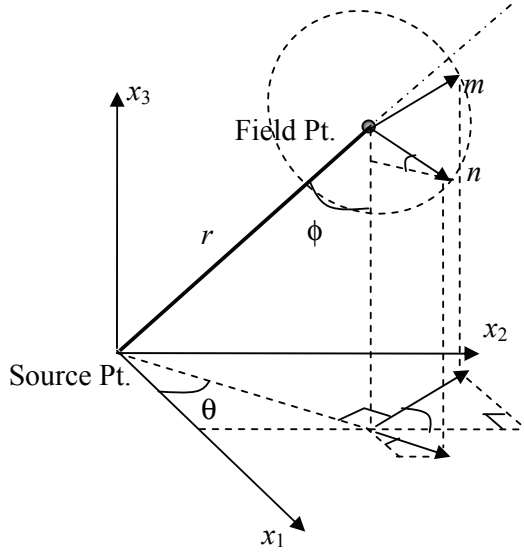By introducing the following three tensors (Ting, 1996),

$$Q \equiv Q_{ik} = C_{ijks}n_jn_s, \quad R \equiv R_{ik} = C_{ijks}n_jm_s, \quad T \equiv T_{ik} = C_{ijks}m_jm_s, \qquad (6)$$

eq. (5) can be rewritten into a simple form,

$$\mathbf{Z}(\psi) = \cos^2\psi\mathbf{\Gamma}(p), \qquad (7)$$

where $p = \tan\psi$, and the matrix $\mathbf{\Gamma}(p)$ is given by

$$\mathbf{\Gamma}(p) = \mathbf{Q} + p(\mathbf{R} + \mathbf{R}^T) + p^2\mathbf{T}. \qquad (8)$$

Figure 1: Definition of the unit vectors **n**, **m**

By letting $\mathbf{V} = (\mathbf{R} + \mathbf{R}^T)$, eq. (8) may be rewritten as

$$\boldsymbol{\Gamma}(p) = \mathbf{Q} + p\mathbf{V} + p^2\mathbf{T}. \tag{9}$$

A sextic equation in p is obtained by setting the determinant, $|\boldsymbol{\Gamma}(p)|$, to zero, the six independant roots of which are the Stroh's eigenvalues. These roots must be complex for positive strain energy, and they appear as three pairs of complex conjugates. It can be proved (Hagedorn, 2000) that the sextic equation is not analytically tractable, however the computational effort to obtain the roots, such as by the Laguerre method, is not overly demanding.

By defining a matrix, $\mathbf{H}[\mathbf{x}]$, which depends only on the direction of $\mathbf{x}$ and not its magnitude (the notation $[\mathbf{x}]$ instead of $(\mathbf{x})$ in the term is used for this reason), as

$$\mathbf{H}[\mathbf{x}] = \frac{1}{\pi} \int_0^\pi \mathbf{Z}^{-1}(\psi)d\psi, \tag{10}$$

the Green's displacements can be expressed as

$$U(\mathbf{x}) = \frac{1}{4\pi r}\mathbf{H}[\mathbf{x}]. \tag{11}$$

$\mathbf{H}[\mathbf{x}]$ is the Barnett-Lothe tensor and it remains symmetric and positive definite on an oblique plane; hence, so is the Green's function $U(\mathbf{x})$. By writing the complex

roots as

$$p_v = \alpha_v + i\beta_v, \beta_v > 0, (v = 1,2,3),\tag{12}$$

where both α_v and β_v are real, Ting and Lee (1997) has further shown that $\mathbf{H}[\mathbf{x}]$ can be expressed as

$$\mathbf{H}[\mathbf{x}] \equiv H_{ij} = \frac{1}{|\mathbf{T}|} \sum_{n=0}^{4} q_n \hat{\Gamma}^{(n)},\tag{13}$$

and q_n is given by

$$q_n = \begin{cases} \frac{-1}{2\beta_1\beta_2\beta_3} \left[Re \left\{ \sum_{t=1}^{3} \frac{p_t^n}{(p_t - \bar{p}_{t+1})(p_t - \bar{p}_{t+2})} \right\} - \delta_{n2} \right] & \text{for } n = 0,1,2, \\ \frac{-1}{2\beta_1\beta_2\beta_3} \left[Re \left\{ \sum_{t=1}^{3} \frac{p_t^{n-2} \bar{p}_{t+1} \bar{p}_{t+2}}{(p_t - \bar{p}_{t+1})(p_t - \bar{p}_{t+2})} \right\} \right] & \text{for } n = 3,4 \end{cases}\tag{14}$$

In eq. (14), the subscript t follows the cyclic rule $t = (t-3)$ if $t>3$; $\hat{\Gamma}$ is the adjoint of Γ which can be shown to be a polynomial in p of degree four; and the over-bar in $\bar{p}$ denotes the complex conjugate. Also, $\mathbf{Re}\{\}$ represents the operation of taking real part, and δ_{mn} is the Kronecker delta. The components of $\hat{\Gamma}^{(n)}$, namely, $\hat{\Gamma}_{ij}^{(n)}$, may then be expressed as (Shiah *et al.*, 2008a, b)

$$\hat{\Gamma}_{ij}^{(n)} = \tilde{\Gamma}_{(i+1)(j+1)(i+2)(j+2)}^{(n)} - \tilde{\Gamma}_{(i+1)(j+2)(i+2)(j+1)}^{(n)}, \quad (i,j = 1, 2, 3),\tag{15}$$

after some basic algebraic manipulation, and the 4-order tensor $\tilde{\Gamma}^{(n)}$ can be shown to be given by

$$\begin{aligned}
\tilde{\Gamma}_{pqrs}^{(4)} &= T_{pq}T_{rs}, \\
\tilde{\Gamma}_{pqrs}^{(3)} &= V_{pq}T_{rs} + T_{pq}V_{rs}, \\
\tilde{\Gamma}_{pqrs}^{(2)} &= T_{pq}Q_{rs} + T_{rs}Q_{pq} + V_{pq}V_{rs}, \\
\tilde{\Gamma}_{pqrs}^{(1)} &= V_{pq}Q_{rs} + V_{rs}Q_{pq}, \\
\tilde{\Gamma}_{pqrs}^{(0)} &= Q_{pq}Q_{rs}.
\end{aligned}\tag{16}$$

The calculations involved in eqs. (13)-(16) to obtain $\mathbf{U}(\mathbf{x})$ using eq.(11) are relatively straightforward; the only numerical approach required in any of the steps is for the solution of the sextic equation for p.

The numerical evaluation of the fundamental solution for tractions T_{ij}^* is also required. This may be carried out using

$$T_{ij}^* = (\sigma_{ik}^* N_k)_j,\tag{17}$$

where σ_{ik}^* is the fundamental solution for stresses at a field point due to a concentrated force applied in the x_j direction at the source point, and N_k is the outward normal vector on the surface at the field point. These stresses, denoted also by $\boldsymbol{\sigma}_j^*$ here, can be determined using the generalized Hooke's law, as follows,

$$\boldsymbol{\sigma}_j^* = \mathbf{C}\boldsymbol{\varepsilon}_j^*, \tag{18}$$

where

$$\boldsymbol{\sigma}_l^* = (\sigma_{11}^*, \ \sigma_{22}^*, \ \sigma_{33}^*, \ \sigma_{23}^*, \ \sigma_{13}^*, \ \sigma_{12}^*)_l^T, \tag{19}$$

$$\boldsymbol{\varepsilon}_l^* = (\varepsilon_{11}^*, \ \varepsilon_{22}^*, \ \varepsilon_{33}^*, \ 2\varepsilon_{23}^*, \ 2\varepsilon_{13}^*, \ 2\varepsilon_{12}^*)_l^T, \tag{20}$$

In eq. (20), the strains $(\varepsilon_{ik}^*)_j$ are computed using the strain-displacement relations:

$$(\varepsilon_{ik}^*)_l = \left(U_{il,j} + U_{jl,i}\right)/2. \tag{21}$$

In this paper, the analytically exact, explicit expression of the derivatives of U_{ij} as obtained by Lee (2003), following the work in Ting and Lee (1997), is adopted. The first derivative of U_{ij} can be written as follows (Lee, 2003; Shiah *et al.*, 2008b):

$$U_{ij,l} = \frac{1}{4\pi^2 r^2} \left[-\pi y_l H_{ij} + C_{pqrs}\left(y_s M_{lqiprj} + y_q M_{sliprj}\right)\right] \tag{22}$$

In eq. (22), y_i are the components of the unit position vector $\mathbf{y} = \frac{\mathbf{x}}{r}$ in a spherical coordinate system and are given by

$$y_1 = \sin\phi\cos\theta, \quad y_2 = \sin\phi\sin\theta, \quad y_3 = \cos\phi. \tag{23}$$

Furthermore, the explicit expression of M_{ijklmn} is given in terms of the Stroh's eigenvalue p_t as

$$M_{ijklmn} = \frac{2\pi i}{|T|^2} \sum_{t=1}^{3} \frac{1}{(p_t - p_{t+1})^2 (p_t - p_{t+2})^2}$$
$$\left[\Phi'_{ijklmn}(p_t) - 2\Phi_{ijklmn}(p_t) \times \left(\frac{1}{p_t - p_{t+1}} + \frac{1}{p_t - p_{t+2}}\right)\right], \quad (24)$$

in which the prime denotes differentiation of Φ with respect to the argument p; and the function $\Phi_{ijklmn}(p)$ can be shown to be

$$\Phi_{ijklmn}(p) = \frac{B_{ij}(p)\,\hat{\Gamma}_{kl}(p)\hat{\Gamma}_{mn}(p)}{(p - \bar{p}_1)^2 (p - \bar{p}_2)^2 (p - \bar{p}_3)^2}, \tag{25}$$

where $B_{ij}(p)$ is given by

$$B_{ij}(p) = n_i n_j + (n_i m_j + m_i n_j)\, p + m_i m_j p^2. \tag{26}$$

In eq. (24), p_{t+1} and p_{t+2} follow the cyclic rule for $t > 2$ as indicated earlier. It should perhaps also be mentioned that it is not necessary to rewrite the term $\Phi'_{ijklmn}(p_t)$ as a fully explicit expression, since it is a relatively simple matter to program the functions $B(p)$, $\hat{\Gamma}(p)$, $(p - \bar{p}_t)^2$ and their derivatives into subroutines in the computer code and then apply the chain rule in the differentiation. Although eq. (24) appears to be in a complex form, its imaginary part will eventually disappear to yield real variables. It should be mentioned that, unlike eq. (13), eq. (24) becomes invalid when repeated roots of the sextic equation occurs (i.e. $p_t = p_{t+1}$ or $p_t = p_{t+1} = p_{t+2}$). However, this situation is not commonly encountered, occurring only for specific field points of materials with very particular properties. A simple way to overcome this problem if it happens is to introduce a small perturbation to one of the repeated roots when computing eq. (24). Work to resolve this issue analytically remains ongoing.

3   Numerical implementation

The above fundamental solutions have been implemented into a conventional 3D BEM code which was developed previously for the solution of the corresponding BIE, eq. (1), for 3D isotropic elastostatics. It is based on the quadratic isoparametric element formulation in which 8-node quadrilateral and 6-node triangular elements are used. The numerical algorithm in this regard for anisotropic elasticity is the same as for the case of isotropy. Thus, the necessary modifications to the code pertain primarily to the material properties and the evaluation of the fundamental solutions. Due to their explicit algebraic forms, the latter are relatively easy to implement; indeed, this is an important merit of the present algorithm. For the numerical evaluation of the high-order tensors in the formulation, it is also expedient to exploit the symmetry property of these tensors which significantly reduces the computational effort in their numerical evaluations.

In the formation of the system equations, integration of the terms involving the displacement and traction fundamental solutions is carried out over each boundary element in turn using standard quadrature. No special adaptive scheme was employed here, and the numerical integration is carried out with standard 4×4 Gauss quadrature for quadrilateral elements and 13-point Hammer-Stroud quadrature for triangular elements. At each field point, the sextic equation, which arises from equating to zero the determinant of the matrix in eq. (9), is solved numerically for the Stroh's eigenvalues. The accuracy and efficiency of computing the

Green's displacements and stresses depend to a significant extent on the numerical solution of this equation. In the present work, Laguerre's method is employed for the numerical solution of the sextic equation. It is generally accepted as one of the most straightforward and simple methods with which convergence of solution is guaranteed (see, e.g., Press *et al.*, 1990). The process is usually accompanied by the use of polynomial deflation whereby the polynomial is factored into a product involving the root and a reduced polynomial of degree one less than the original. A possible modification of Laguerre's method to enhance the efficiency of the sextic equation solution is to compute first, one pair of conjugate roots; the reduced 4th degree polynomial can perhaps then be solved analytically. It should however be remarked here that no attempt is made in the present study to evaluate and quantitatively assess the computational efficiency of the implemented algorithm; the primary focus has hitherto been to establish its correctness and integrity. It should also be reminded that repeated roots or closely-spaced roots may pose difficulties for the Green's function for the stresses used here. In the general case, it is not possible to establish the pathology displayed by repeated roots from simply examining the coefficients of the sixth-degree polynomial. In practice, the difficulties associated with repeated roots can be easily overcome by introducing a small perturbation to one of the repeated roots as mentioned earlier.

4   Numerical examples

Three numerical examples are presented here to demonstrate the veracity of the formulations implemented and the application of the BEM to three-dimensional stress analysis in anisotropic elasticity. As an initial check of the BEM models employed for these problems, the established BEM code for isotropy was first used to solve each of them using isotropic material properties. The analysis was repeated using the implemented anisotropic algorithm; identical numerical results were obtained in all cases. The first example considered, *Problem A*, is a rectangular prism of alumina crystal (Al_2O_3) subjected to pure shear for which an exact analytical solution of the displacements has been derived by Lekhnitskii (1963). In *Problem B*, the stress distributions around a spherical cavity and in a hollow sphere subjected to remote hydrostatic stress are determined. The problem of a cylindrical bar with a spherical cavity and under remote tension is then analyzed in the last example, *Problem C*. Using Eshelby's equivalent inclusion method, Chiang (2007) has investigated the stress concentrations around a spherical cavity in an infinite cubic medium under different uniform loading conditions; his solutions are used for comparison with the present BEM results in *Problems B* and *C* using the properties of niobium (*Nb*) crystal which is cubic. In the analysis of these problems, the principal material axes of the crystals are taken be coincide with the global Carte-

sian axes, unless indicated otherwise. In *Problem C*, additional analyses involving rotations of the principal material axes were further carried out as will be explained later. These were done solely for the purpose of further demonstrating the suitability of the present BEM program to treat fully general anisotropic materials. The elastic constants (stiffness coefficients) for the *Nb* and *Al$_2$O$_3$* crystals are taken to be as follows (Huntington, 1958):

For *Nb* crystal, C_{11}= 246 GPa; C_{12}= 134 GPa; C_{44}= 28.7 GPa.

For *Al$_2$O$_3$* crystal, C_{11}= 465 GPa; C_{33}= 563 GPa; C_{44}= 233 GPa; C_{12}= 124 GPa; C_{13}= 117 GPa; C_{14}= 101 GPa.

4.1   Problem A

Figure 2 shows a rectangular alumina crystal parallelepiped which is subjected to a unit uniform shear stress $\tau_{23} = \tau_o$= 1 on four of its sides. The BEM mesh employed is shown in Fig.3; it has 10 quadrilateral elements and 32 nodes. To preclude rigid body motion in the analysis, the node at the origin was fully constrained, while that at coordinates (0, 0, 3a) was fixed in the x_1- and x_2-directions; all the other (mid-side) nodes in the x_1= 0 plane are also restrained in the x_1-direction. The displacements, u_i, obtained from the present BEM analysis at the five points A – E indicated in Fig. 2 are listed in Table 1. The numerical values are compared with those calculated using Lenitskii's (1963) exact analytical solution, where it can be seen that there is excellent agreement between the two sets of results.

Table 1: Displacements, u_i, at points A – E in *Problem A*.

| Point	Result	u_1	u_2	u_3
A (-0.5, -1.0 , 1.0)	BEM	0.85546E-3	-0.17105E-2	-0.57737E-2
	Exact	0.85519E-3	-0.17104E-2	-0.57747E-2
B (0.5, 0.0 , 1.0)	BEM	-0.85530E-3	0.10165E-6	0.67901E-6
	Exact	-0.85519E-3	0	0
C (0.5, 1.0 , 1.0)	BEM	-0.85533E-3	0.17105E-2	0.57747E-2
	Exact	-0.85519E-3	0.17104E-2	0.57747E-2
D (-0.5, -0.5 , 0)	BEM	0.85533E-3	-0.85585E-3	-0.28864E-2
	Exact	0.85519E-3	-0.88519E-3	-0.28874E-2
E (-0.5, 1.0 , 0.5)	BEM	0.85499E-3	0.17105E-2	0.57748E-2
	Exact	0.85519E-3	0.17104E-2	0.57747E-2
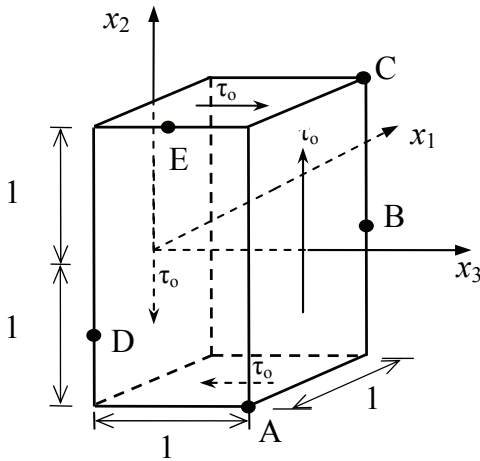
Figure 2: A rectangular alumina crystal prism under uniform shear stress: *Problem A*
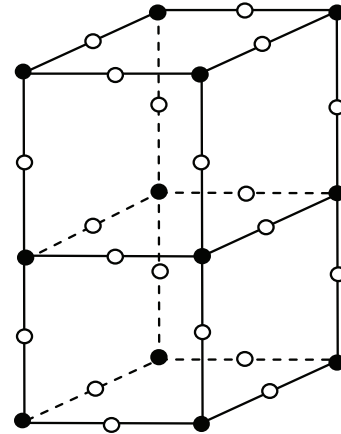
Figure 3: BEM mesh for *Problem A* : 10 elements, 32 nodes

4.2 Problem B

In the second example, the stress distributions at the inner and outer surfaces of a thick-walled sphere subjected to uniform hydrostatic tensile stress, σ_o, at the outer surface are determined for a cubic material. Referring to Fig. 4, the radius ratios considered were $K = R_2/R_1 = 1.5$, 2, 3, 4 and 20. The same basic mesh design shown in Fig. 5 and the material properties of niobium crystal were used in the BEM analysis; the BEM mesh contains a total of 64 elements and 156 nodes, the exterior surface being modeled with just 16 triangular elements with 34 nodes. It should be remarked that advantage can be taken of the symmetry of the material properties for the cubic medium and the loading conditions, and only a fraction of the physical problem needs to be modeled. However, the whole sphere was modeled to establish the suitability of the mesh design which can then be employed for more general anisotropic properties in future studies. Table 2 lists the computed normalized stresses, $k_\theta = \sigma_\theta/\sigma_o$ and $k_z = \sigma_\phi/\sigma_o$, at the four nodal points along the inner surface of the sphere in the plane of the "horizontal" equator (i.e. in the x_1-x_2). Also shown in the table are the corresponding analytical solution and BEM results using the same mesh for the case of isotropy; it is evident that the anisotropic material properties has a significant influence on the stress distributions in the sphere. Unlike in isotropy, the direct stresses σ_θ and σ_ϕ are no longer of the same magnitude in the sphere of *Nb* crystal under the hydrostatic stress loading. A

comparison of the BEM results for the case of $R_2/R_1 = 20$ with Chiang's (2007) analytical solution can be made; the errors introduced by the finite external radius in the BEM analysis for this case are not expected to be significant. The deviations between the two sets of results at the nodal points are all within 1.0% for k_z and 1.5% for k_θ, demonstrating the veracity and accuracy of the present formulation.
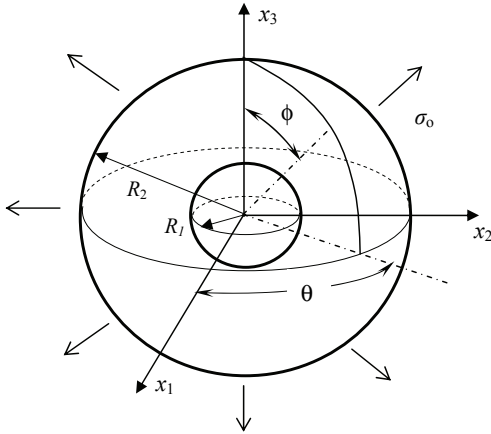

Figure 4: A thick-walled sphere subject to remote hydrostatic stress, σ_o- *Problem B*
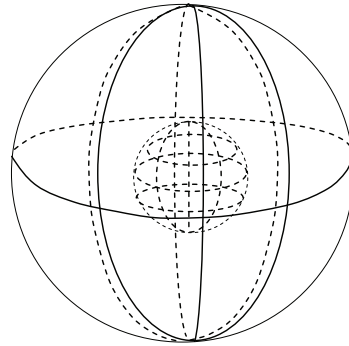

Figure 5: BEM mesh for the case of $K = 2$, *Problem B*: 64 elements, 156 nodes

4.3   *Problem C*

The third example considered is a cylindrical bar with a spherical cavity under remote tension, σ_o, as shown in Figure 6. The range of cavity sizes considered was $a/R = 0.1$ to 0.5, where a and R are the radii of the cavity and the cylindrical bar, respectively; also, the half-length of the bar $H = 2R$. A typical BEM mesh used is shown in Figure 7; the same basic mesh configuration was used in all cases of a/R. The problem was first solved for a cubic medium where a check of the results for the case of $a/R = 0.1$ can be made with the solution by Chiang (2007) for an infinite body using the properties of *Nb* crystal. Table 3 shows the computed BEM results of the normalized stresses, $k_z = \sigma_{33}/\sigma_o$ and $k_\theta = \sigma_\theta/\sigma_o$, around the horizontal equator for a niobium crystal cylindrical bar with the spherical cavity. A comparison of the BEM anisotropic results and Chiang's (2007) solution is also shown. Again, excellent agreement was obtained between the two sets of results; the deviations for k_z were all within 1.0% while those for the significantly smaller magnitudes of k_θ were less than 3.0%.

Table 2: Normalized stresses, $k_\theta = \sigma_\theta/\sigma_o$ and $k_z = \sigma_\phi/\sigma_o$, around the equator about the x_3-axis (i.e. in the x_1-x_2 plane) of a spherical cavity in *Nb* crystal hollow sphere subjected to hydrostatic tensile stress σ_o at the external radius: *Problem B*.

R_2/R_1	Normalized Stresses	Isotropic Solution	Anisotropic Solution			
			$\theta = 0°$	$\theta = 15°$	$\theta = 30°$	$\theta = 45°$
20	k_z	1.4965 (BEM)	2.0083 (*2.0221)	1.9094 (*1.9109)	1.7662 (*1.7688)	1.7163 (*1.7203)
	k_θ	1.5002 (Exact)	2.0083 (*2.0221)	1.6886 (*1.7066)	1.2886 (*1.3037)	1.1521 (*1.1657)
4	k_z	1.5228 (BEM)	2.0365	1.9342	1.7894	1.7387
	k_θ	1.5238 (Exact)	2.0365	1.7204	1.3184	1.1800
3	k_z	1.5597 (BEM)	2.0638	1.9635	1.8186	1.7676
	k_θ	1.5580 (Exact)	2.0638	1.7564	1.3609	1.2217
2	k_z	1.7257 (BEM)	2.2720	2.1507	2.0021	1.9628
	k_θ	1.7143 (Exact)	2.2381	1.9216	1.5472	1.4245
1.5	k_z	2.1546 (BEM)	2.5440	2.3844	2.3046	2.2922
	k_θ	2.1316 (Exact)	2.4920	2.2772	1.9169	1.8349

* Numerical solution in Chiang (2007) for $R_2 = \infty$; results at $\theta=15°$ are interpolated from his tabulated values

Table 3: Stress concentration around the equator about the x_3-axis of a spherical cavity in a *Nb* crystal cylindrical bar subjected to remote tension σ_o: *Problem C*; $k_\theta = \sigma_\theta / \sigma_o$ and $k_z = \sigma_{33} / \sigma_o$

a/R	Stress Concentration	Anisotropic Solution			
		$\theta = 0°$	$\theta = 15°$	$\theta = 30°$	$\theta = 45°$
0.1	k_z	2.4910 (*2.4958)	2.4729 (*2.4767)	2.4488 (*2.4523)	2.4410 (*2.4439)
	k_θ	0.3389 (*0.3481)	0.2870 (*0.2863)	0.2188 (*0.2244)	0.1961 (*0.2007)
0.2	k_z	2.5043	2.4865	2.4626	2.4455
	k_θ	0.3328	0.2844	0.2147	0.1923
0.3	k_z	2.5453	2.5275	2.5039	2.4964
	k_θ	0.3215	0.2707	0.2045	0.1828
0.4	k_z	2.6048	2.5901	2.5672	2.5605
	k_θ	0.3005	0.2544	0.1881	0.1657
0.5	k_z	2.7733	2.7574	2.7327	2.7260
	k_θ	0.2827	0.2337	0.1658	0.1391

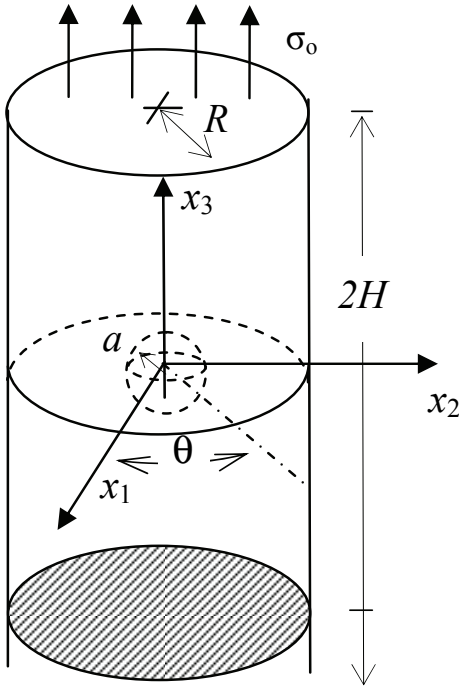* Numerical solution in Chiang (2007) for R=∞; results at θ=15° are interpolated from his tabulated values.

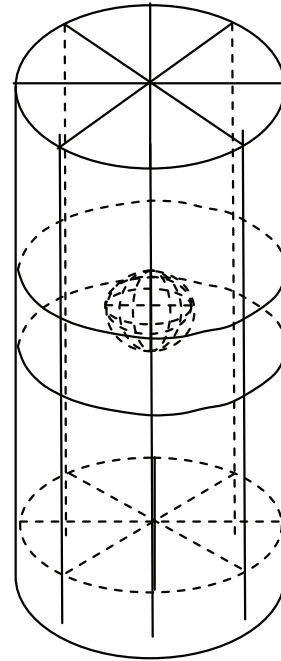Figure 6: A cylinder with a spherical cavity under remote tension- *Problem C*

Figure 7: Typical BEM mesh of the cylinder for *Problem C*: 88 elements; 288 nodes

For the same cylindrical bar made of alumina crystal under the remote tension, the computed stress concentration factor was found to be uniform around the horizontal equator at the surface of the cavity. Figure 8 shows the variation of the stress concentration factor, $k_z = \sigma_{33}/\sigma_o$, for the various a/R ratios considered. Also shown for comparison are the results obtained using ANSYS FEM analysis, where it can be see that there is excellent agreement between them; a typical FEM mesh employed is shown in Fig. 9. For isotropy, the stress concentration factors are dependent on the Poisson's ratio; the results for the case of Poisson's ratio of 0.3 are plotted in Fig. 8 as well. Interestingly, the deviations of corresponding values of k_z between the anisotropic and isotropic cases are relatively small. In addition, the magnitudes of σ_θ/σ_o are typically two orders of magnitude smaller than k_z,

and hence are not presented here. This is not too surprising in view of the near quasi-isotropy in the x_1-x_2 plane.

As a demonstration of the applicability of the BEM program to treat full general anisotropy, the principal material axes in the x_1-, x_2- and x_3-directions of the alumina are rotated clockwise by 30°, 45° and 60°, respectively. These rotations are arbitrarily chosen; they result in a fully populated stiffness matrix in the Cartesian coordinate system for the physical problem as follows:

$$[C] = \begin{bmatrix} 544.8 & 153.6 & 57.3 & 10.5 & 65.7 & -81.2 \\ 153.6 & 531.1 & 28.4 & -14.7 & -18.1 & 89.7 \\ 57.3 & 28.4 & 654.4 & 19.8 & -6.4 & 10.4 \\ 10.5 & -14.7 & 19.8 & 106.4 & 24.8 & 13.3 \\ 65.7 & -18.1 & -6.4 & 24.8 & 167.9 & 22.5 \\ -81.2 & 89.7 & 10.4 & 13.3 & 22.5 & 243.5 \end{bmatrix} \tag{27}$$

The BEM analysis was repeated for all the cases of a/R treated above, and the ANSYS FEM analysis was also carried out for comparison of the results. It was found that even with the rotation of the three principal material axes, the stress concentration factor k_z does not vary significantly around the horizontal equator of the spherical cavity, with the deviations of the nodal values from one another being less than 2.5% for all the geometries analyzed. Thus it may, for all intents and purposes, be considered to be also uniform. The variation of k_z with a/R is also shown in Fig. 8. What is clearly evident is the elevation of its magnitude with the change in orientations of the material axes. The BEM and FEM results again show very good agreement indeed.

5   Conclusions

A BEM formulation based on closed-form algebraic expressions of the fundamental solutions for the elastostatic three-dimensional stress analysis of solids with general anisotropy has been presented in this paper. These Green's functions have been derived by Ting and Lee (1997) and Lee (2003) and are expressed in terms of Stroh's eigenvalues; they have never been previously employed in BEM formulations for general anisotropy. Their explicit algebraic forms allow relatively simple implementation into an existing BEM code which had been developed for 3D isotropic elasticity. Three example problems have been presented to illustrate the veracity of the numerical implementation. They include those with stress concentrations for which the BEM is well known to be very well suited to treat. Where possible, the numerical results obtained from the BEM analysis have been compared with known solutions in the literature or with those obtained by the finite element method, and very good agreement between them have been obtained.
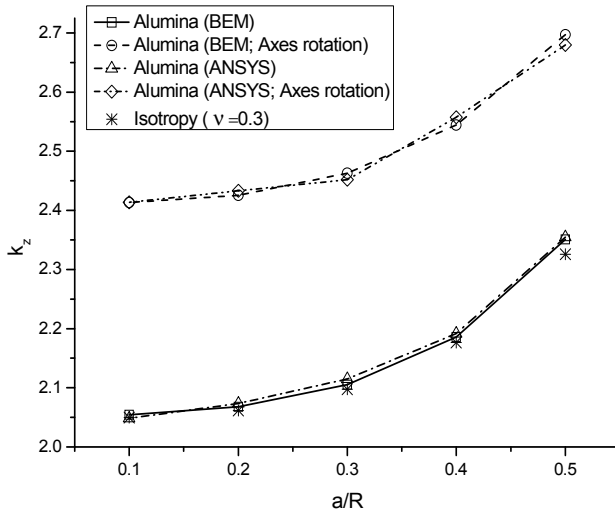
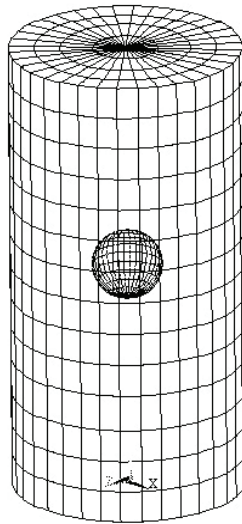Figure 8: Variation of the stress concentration factors with a/R- *Example C*

Figure 9: Finite Element meshes in ANSYS (2940 SOLID5 elements; 6826 nodes)- *Example C*

References

Aliabadi, M.H. (2002): *The Boundary Element Method: Volume 2 Applications in Solids and Structures.* John Wiley & Sons, Chichester, England.

Barnett, D.M. (1972): The precise evaluation of derivatives of the anisotropic elastic Green's functions. *Phys. Stat. Sol.* (b) 49, 741–748.

Chen, T.; Lin, F.Z. (2001): Numerical evaluation of derivatives of the anisotropic elastic Green's functions. *Mech. Res. Comm.*, 20, 501-506.

Chiang, C.R. (2007): Stress concentration around a spherical cavity in a cubic medium, *J. Strain Analysis*, 42, 155-162.

Hagedorn, T.R. (2000): General formulas for solving solvable sextic equations. *J. Algebra*, 233, 704-757.

Huntington, H.B. (1958): *The Elastic Constants of Crystal.* Academic Press, New York.

Lee,V.G. (2003): Explicit expression of derivatives of elastic Green's functions for general anisotropic materials. *Mech. Res. Comm.*, 30, 241–249.

Lenitskii, S.G. (1963): *Theory of Elasticity of an Anisotropic Body.* Holden-Day Publishers, San Francisco.

Li, S.; Atluri, S.N. (2008)**:** The MLPG mixed collocation method for material orientation and topology optimization of anisotropic solids and structures, *CMES: Computer Modeling in Engineering & Sciences*, 30, 37-56.

Lifshitz, I.M.; Rozenzweig, L.N. (1947): Construction of the Green tensor for the fundamental equation of elasticity theory in the case of unbounded elastically anisotropic medium, *Zh. Eksp. Teor. Fiz.*, 17, 783-791.

Liu, G.R.; Achenbach, J.D. (1994): A strip element method for stress analysis of anisotropic linearly elastic solids, *Trans. ASME J. Appl. Mech.*, 61, 270-277.

Nakamura, G.; Tanuma, K. (1997): A formula for the fundamental solution of anisotropic elasticity. *Q. J. Mech. Appl. Math.*, 50, 179-194.

Paik, H.S.; Lee, S.Y. Chang, S.Y. (2004): Finite difference stress analysis of anisotropic three-dimensional curved bodies with free boundaries, *KSCE J. Civil Engng.*, 8, 49-57.

Pan, E.; Yuan, F.G. (2000): Boundary element analysis of three dimensional cracks in anisotropic solids. *Int. J. Numer. Methods Engng.*, 48, 211-237.

Phan, P.V.; Gray, L.J.; Kaplan, T. (2004): On the residue calculus evaluation of the 3D anisotropic elastic Green's function. *Comm. Numer. Methods Engng.*, 20, 335-341.

Sales, M.A.; Gray, L.J. (1998): Evaluation of the anisotropic Green's function and its derivatives. *Comp. & Struct.*, 69, 247-254.

Shiah, Y.C.; Tan, C.L. (2000): Fracture mechanics analysis in 2D anisotropic thermoelasticity using BEM, *CMES: Computer Modeling in Engineering & Sciences*,

1, 91-99.

Shiah, Y.C.; Guao, T.L.; Tan, C.L. (2005): Two-dimensional BEM thermoelastic analysis of anisotropic media with concentrated heat sources, *CMES: Computer Modeling in Engineering & Sciences*, 7, 321-338.

Shiah, Y.C.; Tan, C.L.; Lee, V.G.; Chen, Y.H. (2008a): Evaluation of Green's functions for 3D anisotropic elastic solids. *Advances in Boundary Element Techniques IX*, *Proc. BeTeq 2008 Conf.*, *Seville*, R. Abascal & M.H. Aliabadi (eds.), E.C. Ltd. (U.K.), pp. 119-124.

Shiah, Y.C.; Tan, C.L.; Lee, V.G. (2008b): Evaluation of explicit-form fundamental solutions for displacements and stresses in 3D anisotropic elastic solids. *CMES: Computer Modeling in Engineering & Sciences*, 34, 205-226.

Sladek, J.; Sladek, V.; Atluri, S.N. (2004): Meshless local Petrov-Galerkin method in anisotropic elasticity, *CMES: Computer Modeling in Engineering & Sciences*, 6, 477-489.

Synge, J.L. (1957): *The Hypercircle in Mathematical Physics*, Cambridge University Press, Cambridge.

Tan, C.L. (1983): Boundary integral equation stress analysis of a rotating disc with a corner crack. *J. Strain Analysis Engng. Design*, 18, 231-237.

Tan, C.L.; Gao, Y.L. (1992): Boundary element analysis of plane anisotropic bodies with stress concentrations and cracks, *Composite Struct.*, 20, 17-28.

Tan, C.L.; Gao, Y.L.; Afagh, F.F. (1992): Anisotropic stress analysis of inclusion problems using the boundary integral equation method, *J. Strain Analysis Eng'ng Design*, 27, 67-76.

Tan, C.L.; Fenner, R.T. (1978): Three dimensional stress analysis by the boundary integral equation method. *J. Strain Analysis Eng'ng Design*, 13, 213-219.

Tan, C.L.; Fenner, R.T. (1979): Elastic fracture mechanics analysis by the boundary integral equation method. *Proc. Royal Soc. London*, A369, 243-260.

Tavara, L.; Ortiz, J.E; Mantic, V.; Paris, R. (2008): Unique real-variable expressions of displacement and traction fundamental solutions covering all transversely isotropic materials for 3D BEM. *Int. J. Numer. Methods Engng.*, 74, 776-798.

Ting, T.C.T (1996): *Anisotropic Elasticity*, Oxford University Press, Oxford.

Ting, T.C.T.; Lee,V.G. (1997):The three-dimensional elastostic Green's function for general anisotropic linear elastic solid. *Q. J. Mech. Appl. Math.*, 50, 407-426.

Tonon, F.; Pan, E.; Amadei, B. (2001): Green's functions and boundary element method formulation for 3D anisotropic media. *Comp. & Struct.*, 79, 469-482.

Wang, C.Y. (1997): Elastic fields produced by a point source in solids of general

anisotropy. *J. Engng. Math.*, 32, 41-52.

Wang, C.Y.; Denda, M. (2007): 3D BEM for general anisotropic elasticity. *Int. J. Solids Struct.*, 44, 7073-7091.

Wilson, R.B.; Cruse, T.A. (1978): Efficient implementation of anisotropic three dimensional boundary integral equation stress analysis. *Int. J. Numer. Methods Engng.*, 12, 1383-1397.